Self-formed cylindrical microcapillaries through surface migration of silicon and their application to single-cell analysis

2013 J. Micromech. Microeng. 23 055001

(http://iopscience.iop.org/0960-1317/23/5/055001)

IOP Publishing Journal of Micromechanics and Microengineering

J. Micromech. Microeng. **23** (2013) 055001 (9pp) doi:10.1088/0960-1317/23/5/055001

Self-formed cylindrical microcapillaries through surface migration of silicon and their application to single-cell analysis

Fan Zeng[1,2], **Yuan Luo**[1,2], **Levent Yobas**[1,3] **and Man Wong**[1,3]

[1] Department of Electronic and Computer Engineering, The Hong Kong University of Science and Technology, Clear Water Bay, Kowloon, Hong Kong

E-mail: eelyobas@ust.hk and eemwong@ece.ust.hk

Received 21 December 2012, in final form 21 February 2013
Published 21 March 2013
Online at stacks.iop.org/JMM/23/055001

Abstract

Surface migration of monocrystalline silicon has been applied to demonstrate self-formed cylindrical microcapillaries with diameters from 0.8 to 2.8 μm based on the microstructured substrate topography. The microcapillaries are entirely enclosed in silicon and can be conveniently etched to create fluidic access ports and microchannels for their subsequent integration into functional microfluidic devices. Moreover, the microcapillaries can be thermally oxidized through their access ports with silica walls remain intact upon release from surrounding silicon in an effort to enhance optical clarity. Straight microcapillaries and microcapillaries with perpendicular turns and crossings (junctions) have all been fabricated and validated for fluidic continuity with a fluorescein solution pumped through. The utility of the microcapillaries has been showcased on particle traps in which biological cells are probed for single-cell impedance spectroscopy. The approach disclosed, given its full compatibility with semiconductor device fabrication, offers great potential towards intelligent cell and molecule-based devices merging microelectronics and microfluidics.

(Some figures may appear in colour only in the online journal)

1. Introduction

Microfluidics—the manipulation of fluids in channels with dimensions that are tens of micrometers small—has become a major research field, encompassing various disciplines from chemical synthesis and biological analysis to optics and information technology [1]. While a great deal of interest lies in this size regime, there are specific applications that can directly benefit from scaling channel dimensions below a few micrometers—microcapillaries. Microcapillaries, are utilized to position and probe biological cells for their electrical and mechanical characteristics [2–12] and for their treatment by electroporation [13, 14], the technique that enables intracellular delivery of target materials (e.g. nucleic acids, drug compounds). Suction pressure or electric potential applied through microcapillaries draws nearby cells in suspension under field forces and position them at the openings of microcapillaries [15]. Round and smooth openings, in particular silica-based materials, are favored for establishing quality interfaces on cells. Thus, a simple fabrication process capable of producing such round silica-based microcapillaries is highly desired for electrically probing individual cells in microfluidics, the main motivation behind this work. Moreover, such microcapillaries would be beneficial in electrophoretic separation of analytes since they pose extremely high resistance and high surface-to-volume ratio (SVR) capable of suppressing Joule's heating to avert subsequent adverse effects such as band broadening and analyte dispersion [16–18]. In return, higher field strengths can be applied for faster separation and better-resolved isolated bands. Band broadening or analyte dispersion is also an issue when the flow deviates from the characteristic plug profile, typically occurs due to variations in surface potential along microcapillaries [19, 20]. A monolithic microcapillary surrounded by a single substrate is more likely to provide a

[2] Authors equally contributed.
[3] Authors to whom any correspondence should be addressed.

uniform surface potential than those enclosed by a substrate pair [21, 22].

A common method of forming microcapillaries involves bonding a cover plate over a microstructured substrate (e.g. silicon, glass) with a trench profile dry or wet etched upon lithographic patterning [23]. Microstructuring is also performed through replica-moulding methods like casting or hot embossing polymeric materials such as poly(dimethylsiloxane) (PDMS), poly(methyl methacrylate) (PMMA), and poly(carbonate) (PC), among others, using a relief template lithographically prepared [2–4, 8, 11–15]. Depending on the choice of materials, one can apply from a range of bonding techniques including adhesive, eutectic, anodic, and fusion [24]. However, the bonding step is vulnerable to particulates at the interface and needs rigorous cleaning and extreme care to ensure quality [25, 26]. Alternatively, one could avoid bonding by using sacrificial release techniques whereby a thin-film material underneath a structural layer gets entirely removed in an etchant of adequate selectivity to minimize damage to the structural layer. Nevertheless, given the high aspect ratio of a typical microcapillary, this may take hours, compromising the integrity of the structural film due to finite etch selectivity [27, 28].

There are also methods that lead to self-enclosed or buried microcapillaries by enclosing a microstructured trench by subsequent thin-film deposition [5–7, 29–36]. For instance, researchers utilized silicon thermal oxidation and/or deposition of thin-film layers (e.g. SiO_2, Si_3N_4) to seal narrow access windows on top of trenches etched through various methods [29–33]. Moreover, Heuschkel *et al* fabricated microchannels buried in thick liquid and laminated photo-definable polymers for interfacing cultured neural cells [34]. Chuang *et al* extended the technique to stacked microchannels by employing dosage-controlled light exposure and anti-reflection coating between layers [35]. Abbas *et al* used plasma polymerization method to deposit tetramethyldisiloxane (TMDS) layer on trenches photo-defined in a thick resist and obtained rectangular or cylindrical microcapillaries depending on the trench width [36]. Many of these methods, however, have returned microcapillaries either with sub-optimal morphology and surface characteristics or yet to be validated for their capability of electrically probing biological cells. Ong *et al* demonstrated such capability with cylindrical microcapillaries fabricated in a layer of phosphosilicate glass (PSG) over microstructured silicon [5–7]. The method encloses the trench with glass and yet leaves the trench incompletely filled due to a non-conformal deposition profile, thereby trapping a triangular void inside, the precursor of the microcapillary. The triangular void is then transformed into a cylindrical microcapillary in a thermal anneal step which allows the glass filling to reflow and minimize its surface energy. This self-formation of a microcapillary with the desired cylindrical profile, although it is convenient and highly attractive, requires the glass layer to be dry etched to open up the access ports in a subsequent step, which is known to be slow and far less practical than dry etching silicon. Cao *et al* recently addressed this issue with a revised process whereby the access ports self-emerge along with the cylindrical microcapillaries [18]. However, the access ports project a structure in the shape of a funnel and less approachable to biological cells for probing.

Here, we demonstrate self-enclosed cylindrical microcapillaries entirely in bulk silicon based on surface migration of silicon, a phenomenon that is mostly untapped in microfluidic device fabrication. Despite its similarity to thermal reflow in glasses or polymers, silicon surface migration only involves the movement of surface atoms that act to lower the chemical potential associated with the surface curvature [37, 38]. Thus, the crystalline structure of silicon can be preserved. The migration of atoms, when it occurs over length scales comparable to or in excess of structural dimensions, induces a surface topology change leading to a three-dimensional (3D) shape transformation. This principle has been previously applied to reduce sidewall scallops left by deep reactive ion etching, and to create various interesting structures such as microspheres, toroids, and buried voids in silicon [39–44]. A buried spheroid, for instance, can be formed from an isolated rod-like trench that encloses itself under surface migration when annealed in a deoxidizing ambient. Spheroids formed by a series of identical trenches densely populated in a linear array fuse together and create a buried cylindrical microcapillary as schematically described in figure 1(*a*). Microcapillaries can then be integrated into functional microfluidics with reservoirs and microchannels through a lithography-based dry etch (figure 1(*b*)). This etch is relatively straightforward as compared to that of glass microcapillaries since it has to deal with silicon alone. The microcapillaries, once formed, can be thermally oxidized to transform their surfaces into silicon dioxide for electrical and chemical passivation. In the remaining, microcapillaries are investigated for their structural dependence on the initial arrangement of trenches and their ability to form turns and junctions. Their morphology is further uncovered by removing silicon from around their silica walls. Finally, their utility is validated on a device designed for the measurement of a single-cell impedance spectroscopy.

2. Experimental

2.1. Microfabrication

Major fabrication steps are schematically illustrated in figure 2. Silicon wafers (1 0 0)-oriented, p-type, and 100 mm diameter were microstructured with trenches by deep reactive ion etching (DRIE) through a high-resolution photoresist mask (AZ7908) patterned by a stepper (ASML 5000, i-line, exposure energy 290 mW cm^{-2}). Upon stripping off the resist, rapid thermal annealing was performed in argon ambient at 760 Torr 1150 °C for total 4 min (RTP600S). Microchannels and reservoirs were also formed by DRIE applied through a second resist mask aligned and patterned with respect to the first using a contact aligner (MA-6, Karl Suss). Subsequent to the removal of the resist, surface passivation was realized by growing a dry/wet/dry thermal oxide at 1000 °C to a thickness of 600 nm (100/400/100). To provide an extra layer of insulation, a low-temperature oxide (LTO) film 600 nm thick was placed on the

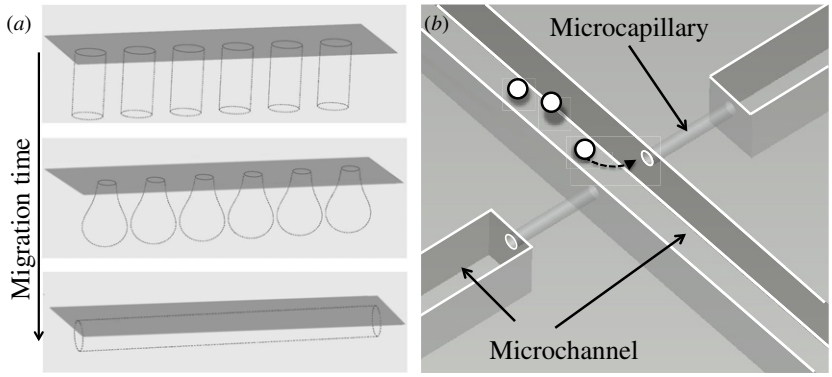

Figure 1. Schematic description of the formation of a self-enclosed microcapillary based on silicon surface migration. (*a*) Rod-like trenches evolve into self-enclosed spheroids, which then fuse together into a pipe-shaped void. (*b*) Conceptual rendering of a microfluidic device integrating microcapillaries and larger microchannels for a specific application, i.e. particle or cell probing.

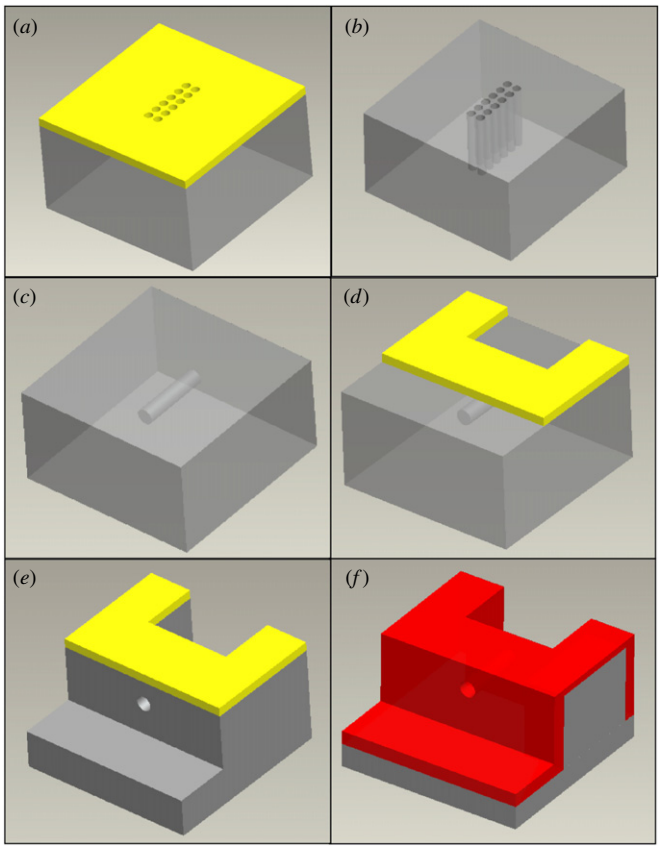

Figure 2. Schematic illustration of key fabrication steps. (*a*) Photolithographic patterning of a resist film (yellow) with an array of fine circular vias. (*b*) DRIE formation of the rod-like trenches followed by the resist strip off. (*c*) Silicon surface migration and evolution of the rod-like trenches into a self-enclosed cylindrical microcapillary. (*d*) Photolithographic patterning of a resist film with coarse features aligned with respect to the microcapillary. (*e*) DRIE formation of the reservoirs and microchannels, exposing the microcapillary on both sides of the silicon partition. (*f*) Surface passivation layer (red) by silicon thermal oxidation and the subsequent LTO deposition.

oxidized wafers in a low-pressure chemical vapor deposition (LPCVD) furnace (420 °C, 180 mTorr). Specimens were prepared for inspection under a scanning electron microscope (SEM, JEOL, JSM-6490). For a more detailed investigation, bulk silicon around some of the microcapillary segments was etched, subsequent to the removal of the top surface oxide, in tetramethylammonium hydroxide (TMAH) solution maintained at 80 °C for 15 min.

2.2. Cell preparation

Human colorectal cancer cells (HCT 116) were cultured in the ATCC-formulated McCoy's 5a (modified) medium supplemented with 10% fetal bovine serum (FBS). The cells were detached from the culture dish using trypsin–EDTA treatment, washed twice (1000 rpm for 8 min) and then resuspended in buffer solution with a composition (in mM): 140 KCl, 2 CaCl2, 2 MgCl2, 20 HEPES, and 10 glucose, adjusted with 300 mM mannitol solution for the conductivity (15 mS cm^{-1}). The cells were fluorescence stained for vitality by incubation in 5 mM Calcein-AM (Life Technologies, Inc., NY). For imaging, microcapillaries were filled with de-ionized (DI) water stained with 1 mM fluorescein under capillary forces.

2.3. Instruments

Microfluidic characterizations were performed on an upright fluorescent microscope (FN1; Nikon, Japan) equipped with a halogen lamp and a mercury lamp (100 W). Images were captured and stored in a computer through a CCD camera (RT3 Mono; SPOT, MI) mounted on the microscope. Electrical measurements were obtained by an impedance analyzer (4294A, Agilent, CA).

2.4. Device preparation

Transparent elastomer covers ∼5 mm thick bored with inlet/outlet ports 3 mm diameter were prepared by casting PDMS (Dow Corning 184) according to the instructions by the manufacturer. The covers were aligned and permanently bonded on the devices fabricated upon their surface activation in oxygen plasma (RF 29W, 1 min, Harrick Plasma). With a syringe-supplied tubing inserted into a fluidic port, all the microchannels and microcapillaries were filled with buffer solution of the same composition as stated above. Impedance

measurements were made across a microcapillary through Ag/AgCl wires placed into the respective ports. Cells were delivered in suspension of the same buffer from a syringe.

3. Results and discussion

Surface migration of silicon atoms takes place at elevated temperatures 900–1300 °C, albeit below the melting point of silicon 1414 °C. It is typically observed in hydrogen ambient over a wide pressure range 10–760 Torr [45], but also reportedly occurs in an ultrahigh vacuum (UHV) environment [46, 47]. Interestingly, however, neither hydrogen nor UHV ambient is absolutely necessary as pointed out by a recent study where migration was encountered in a low-pressure (1 mTorr) non-reducing gas (He, Ne, Ar, N_2) ambient [48]. The study also noticed similar migration rates in noble gases. In an earlier study, 1000 °C anneal in hydrogen at 760 Torr returned a migration rate 600-fold slower than that in argon at the same pressure and 8.2×10^4 fold slower than that in UHV [48]. The results shared here are also from annealing steps performed in argon ambient at 760 Torr.

3.1. Microcapillary diameter

The size of the trenches and their spacing are important design parameters that have direct impact on the diameter of the cylindrical microcapillary to be formed. Such geometrical relations have been previously elucidated in the context of forming a buried void below a thin layer of monocrystalline silicon so as to facilitate low-power high-speed semiconductor devices with minimum parasitic capacitance [39–42]. The pipe-shape voids demonstrated in those studies are typically below 1 μm in diameter and can be further shrunk by subjecting silicon to extended thermal oxidation. Such a fine diameter, although it can be beneficial for nanofluidic devices, is fairly small for other microfluidic applications such as the one described here aiming at a microcapillary for electrical probing of individual cells and thus favors a diameter of a few micrometers. One could increase the opening of a resultant microcapillary by structuring the substrate with larger trenches. Thus, the substrate is structured here with uniform trenches on a one-dimensional (1D) grid that are 6 μm deep and differ in diameter with the values assigned as 0.7, 0.8, and 0.9 all in μm across the designs. Nevertheless, the edge-to-edge separation of the adjacent trenches remains fixed at 0.5 μm, the minimum achievable with our patterning technology. Figure 3(*a*) reveals SEM images of the fabricated designs: those with a trench diameter 0.7 and 0.8 μm lead to microcapillary openings 0.8 and 1.1 μm, respectively, whereas the design with a trench diameter 0.9 μm fails to form a well-defined cylindrical profile. Hence, there appears to be an optimum trench diameter for a given depth that leads to a self-enclosed cylindrical microcapillary with a maximum possible opening. Any further increase in microcapillary opening beyond this point would require a new approach other than merely increasing the diameter of trenches.

The approach adopted here extends the trench pattern to a two-dimensional (2D) grid by repeating the linear pattern of

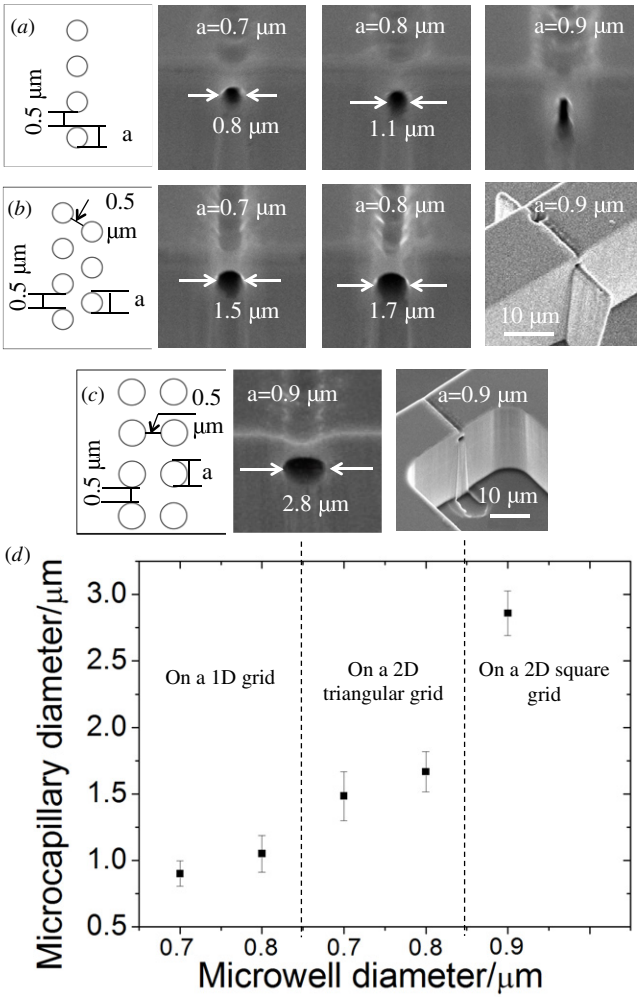

Figure 3. Dimensional dependence of microcapillaries on the size and arrangement of rod-like trenches. (*a*)–(*c*) Layout of uniform trenches structured in silicon for the stated diameters 0.7, 0.8, and 0.9 all in μm and SEM images of associated microcapillary openings exposed on both sides upon integration with microchannels. (*d*) A summary plot with error bars indicating mean $\pm$ 1 standard deviation.

uniform trenches such that their center points coincide on a grid with a unit cell either an equilateral triangle (figure 3(*b*)) or a square (figure 3(*c*)). With trenches 0.7 and 0.8 μm arranged on the triangular grid, microcapillaries are considerably enlarged in diameter as compared to those with trenches of the respective size on the 1D grid. However, trenches 0.9 μm on the triangular grid fail to form self-enclosed microcapillaries and, in return, develop wing structures, artifacts extending both sides of the silicon partition as shown in figure 3(*b*). These artifacts originate from the lithography step during the patterning of the silicon partitions and due to incomplete removal of the resist fill in trenches failed to enclose during annealing. In contrast, when arranged on the square grid, trenches of the same size (0.9 μm) successfully form self-enclosed cylindrical microcapillaries with diameter ~2.8 μm, albeit with a slightly elliptic cross-sectional profile. This can be understood based on the consideration of surface porosity, defined here as the etched fraction of a unit cell footprint. For the triangular and square grids, this fraction

is, respectively, $\pi a^2/2\sqrt{3}\,(a+d)^2$ and $\pi a^2/4\,(a+d)^2$ where a is the diameter of trenches and d is their edge-to-edge separation (0.5 μm). As can be noticed, for a given diameter and separation of trenches, the surface porosity of the substrates structured according to the triangular grid is slightly higher about $2/\sqrt{3} = 1.16$-fold of the porosity of those with the square grid. This causes a slight increase in distance across which silicon atoms must migrate to enclose trenches. According to this definition, per cent porosity of the substrates that leads to successful enclosure of trenches into cylindrical microcapillaries based on the triangular grid arrangement of trenches 0.7 and 0.8 μm is nearly 31% and 34%, respectively. This value exceeds 37% for trenches 0.9 μm and prevents them from being completely enclosed into buried microcapillaries. Rearranging trenches of the same size on the square grid, however, pulls the surface porosity below 33% and allows microcapillaries properly enclosed. Based on this observation, we project that trenches 1.1 μm and beyond on such square grid would similarly fail to enclose, as the surface porosity would exceed 37%.

It should be noticed that the enclosure into a buried microcapillary does not yield a flat surface above the microcapillary with a smooth profile but a slightly indented. This is further exacerbated by the increased porosity of the substrate particularly when it is structured with trenches in the triangular grid arrangement. This could raise a concern over a possible leakage at the interface when a cover plate is mounted on the partition to enclose the remaining microchannels and reservoirs. We believe that this issue can be addressed by performing the anneal step in a low-pressure ambient which is known to induce a smoother surface profile [48].

The results are further summarized in a plot presenting the buried microcapillary diameter as a function of the opening diameter of trenches in figure 3(*d*). With the opening of trenches 0.7–0.9 μm, arranged on the 1D or 2D grids as described earlier, one can obtain cylindrical microcapillaries with diameter values ranging in 0.9–2.8 μm. Beyond this range, smaller microcapillaries would require trenches accordingly smaller, shallower, and more densely packed through a high-resolution lithographic patterning. Larger microcapillaries, in contrast, would make use of trenches proportionally larger, deeper, and further apart. In either case, it is important that the surface porosity be kept below 35% to ensure that microcapillaries can be fully enclosed. Nevertheless, further investigation is needed to determine the practical limit to how large such microcapillaries could be made that is likely to arise from the extended anneal time. As will be verified shortly, these straight microcapillaries are indeed thorough structures fluidically connecting reservoirs on both sides of the partition.

3.2. Routing ability—zigzag microcapillary

Apart from straight microcapillaries, a versatile microfabrication technique should be able to handle turns to realize microcapillary routing in a limited space for a more compact microfluidic design. The routing feature has been put to the test by implementing microcapillaries with a zigzag pattern of reasonably sharp turns (~90°) as detailed in figure 4.

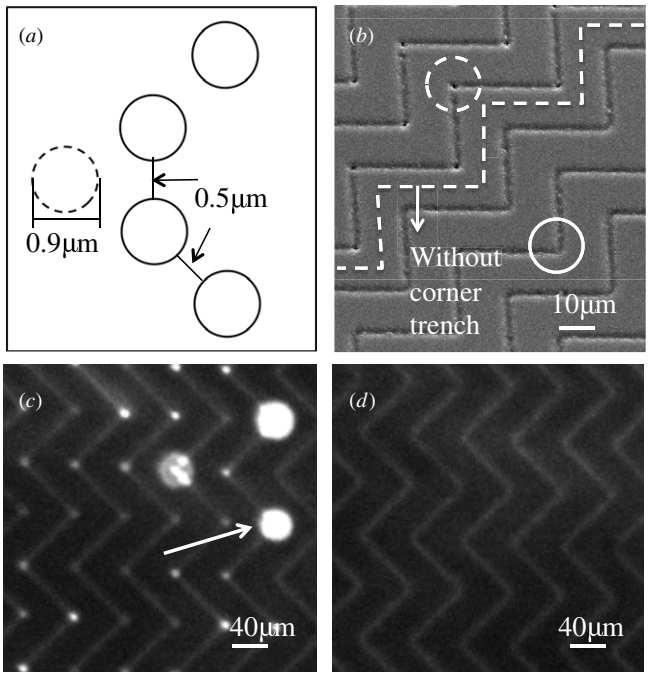

Figure 4. Microcapillary 90° turns: (*a*) Layout of uniform trenches structured around each turn to adjoin straight microcapillaries in perpendicular orientation. The dashed circle refers to the corner trench introduced in some of the designs. (*b*) SEM image of the substrate surface containing microcapillaries with 90° turns. The dashed line demarcates the designs without the corner trench and led to completely enclosed turns (the solid circle) as opposed to those with the corner trench failed to enclose (the dashed circle). (*c*) and (*d*) Fluorescent micrographs imaged upon injecting a fluorescein solution into microcapillaries (*c*) with and (*d*) without the corner trench. The bright spots (e.g. the white arrow) are due to the solution leaked out and accumulated in the corners.

Figure 4(*a*) shows the arrangement of trenches around each turn where a corner trench (the dashed circle) is optionally placed to ensure that succeeding straight segments adjoin. Upon anneal, however, these corner trenches are found with defects and the respective turns are unable to enclose in comparison to those devoid of such corner trench as depicted in the SEM image in figure 4(*b*). These turns expectedly leak when microcapillaries are filled with a fluorescein solution (figure 4(*c*)). In contrast, those without the corner trench are successfully enclosed with no exception. Neither has there been found any turn that leaks nor any microcapillary that is incompletely filled, attesting that the 90° turns devoid of the corner trench are properly formed (figure 4(*d*)). In the images, fluorescence intensity is found to be fairly dim despite the high concentration of fluorescein (1 mM) employed and the extensive exposure time (600 ms) applied for maximum capture of the emission. This is because microcapillaries are buried about 1 μm deep into bulk silicon, which is known to block majority of the visible light [49]. This could pose a serious challenge in many of the microfluidic applications where the optical method of detection is the norm. For those, silicon surface can be selectively etched in a localized region and silica microcapillaries can be exposed to form an optically clear window of detection as presented below. Alternatively, given the compatibility of the platform with

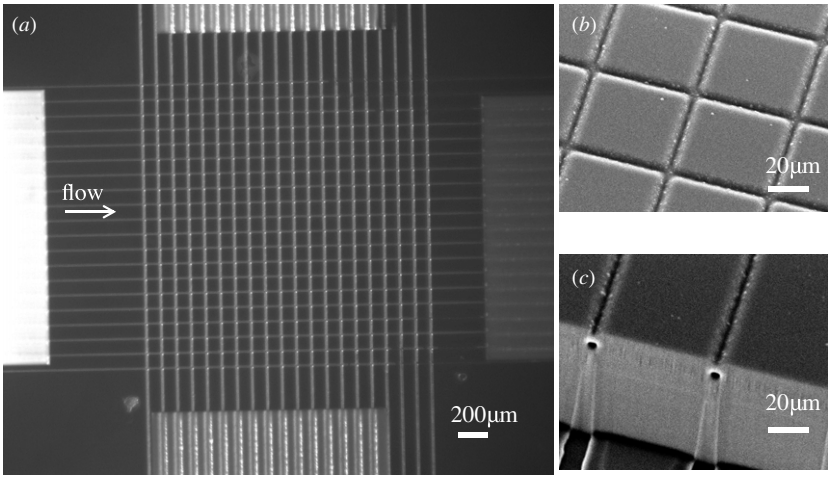

Figure 5. Microcapillary junctions: (*a*) fluorescent micrograph of a network of microcapillaries consists of 400 junctions filled with a fluorescein solution from one side (the arrow). (*b*) and (*c*) SEM images of the distinct sections of the network.

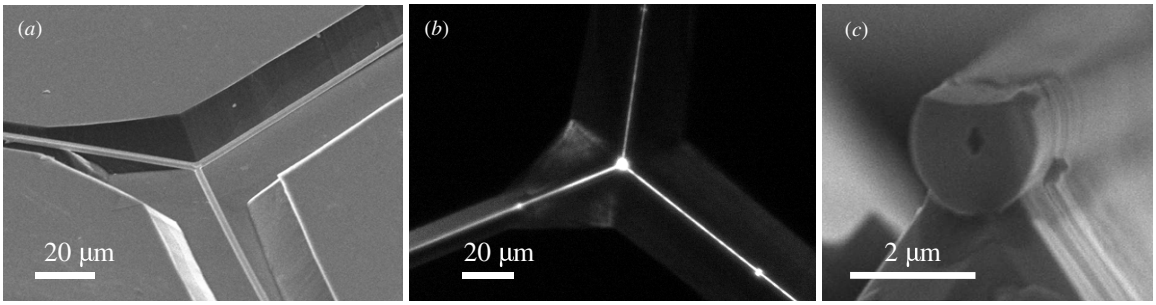

Figure 6. Microcapillary segments exposed upon removal of bulk silicon around their silica walls. (*a*) and (*b*) Y-branch arrangement of three microcapillary segments shown in (*a*) SEM image and (*b*) fluorescent micrograph after being filled with fluorescein solution. (*c*) SEM image of a cross-sectional profile from a microcapillary segment resting on a silicon ridge structure.

microelectronics, microcapillaries can be integrated with electrodes or field-effect devices for electrical or electrochemical detection [50, 51].

3.3. Connectivity—microcapillary junctions

Perhaps the most essential passive component in a functional network of microcapillaries is a simple junction where two or more microcapillaries join together. These junctions are indispensable for serving such functions as mixing or splitting fluids and forming plugs of one fluid in another. Figure 5(*a*) provides a rapid assessment of junctions on a small network of straight microcapillaries (20 × 20) fabricated based on the square-grid arrangement of 0.9 μm trenches (figure 3(*c*)). As shown, fluorescein solution supplied from one end of the rows of microcapillaries fills the entire network with no trace of leakage or blockage in any of the junctions or microcapillary segments. One can notice the slightly higher intensity of emission radiated from the junctions, which can be attributed to their larger volume capacity and the morphology of the substrate surface as can be deduced from the SEM image in figure 5(*b*). While the exact morphology of these junctions has not yet been imaged due to difficulty of sectioning them across, they are expected to project a somewhat ellipsoid shape given the cylindrical profile of the adjoining segments, which is also evident in the microcapillary openings facing a conventional microchannel (figure 5(*c*)).

3.4. Optical access—exposed microcapillary

The layer of monocrystalline silicon formed over microcapillaries is fairly thin and hence unable to entirely block the visible emission emanating from fluorescein solution contained within. However, poor transmission through even such a thin layer can be a handicap in applications dealing with single-molecule imaging or quantitative analysis of analytes enriched or separated through microcapillaries. This issue, as suggested earlier, can be mitigated by selectively removing silicon around microcapillary segments to expose their optically transparent silica walls. However, whether thin silica walls once released could survive residual stresses and preserve their structural integrity has yet to be evaluated. To validate the feasibility of this approach and further investigate the morphology of silica microcapillaires, representative segments released are presented in figure 6. Figure 6(*a*) depicts three microcapillary segments joined in Y-branch configuration suspended over a silicon pit where sidewalls are defined by crystallographic planes emerged from anistropic wet etch. As seen, there is no sign of buckling or fracture noticeable along thin silica walls. The same structure is also

shown after being filled with fluorescein solution (figure 6(*b*)) and the emission received is far more intense than those from buried microcapillaries under comparable conditions (concentration and exposure time). A more detailed view of the morphology can be seen on a cross-sectional profile obtained from a segment resting on silicon and exposed from the sides and the top (figure 6(*c*)). The top appears flat due to overetch during the removal of the surface oxide to expose underneath silicon. Apart from the top, the silica wall of the microcapillary exhibits a cylindrical shell that is about 0.9 μm thick, projecting a diamond-shaped opening 0.5 μm. The shape deviation of the interior from a cylinder could be attributed to stress-limited oxidation and the rate dependence of oxidation on the crystal orientation [52, 53]. For applications where a round opening shape is crucial, reducing oxide thickness could alleviate the issue. These results suggest the viability of the approach for enhancing optical probing of analytes residing in microcapillaries. In addition to optical probing, this could also allow for electrical and thermal probing of a microcapillary content by bringing electrodes or electrolytes in intimate contact with the silica walls. This would be beneficial in applications where field-effect control of flow [54] or temperature regulation of biochemical reactions in microcapillaries is needed [55].

3.5. Application—single-cell impedance spectroscopy

Among various applications, single-cell impedance spectroscopy is pursued here to demonstrate the utility of microcapillaries. We, as well as others, developed single-cell traps in recent years for optical and/or electrical analysis of biological cells on microstructured silicon or polymer substrates, albeit utilizing traditional microfabrication techniques [2–12]. Compared to those, the technique introduced here has certain merits such as convenience and manufacturability as it deals with almost entirely silicon, which is amenable to microstructuring, ability to form cylindrical silica microcapillaries with nearly round openings, a structure-material combination considered ideal for achieving tight grip on biological cells, and compatibility with semiconductor device integration. These traps reside at junctions between microcapillaries and reservoirs or microchannels to which cells can be delivered in suspension. A particular cell of interest is then identified and drawn to the nearby microcapillary opening by suction pressure applied to the respective port. Docking cells is a critical stage during which morphologic and material properties of microcapillary openings could play a determining role towards establishing tight grip on cells and quality electrical recordings. The device and the measurement set up are schematically described in figure 7(*a*). Figure 7(*b*) shows a fluorescent micrograph obtained from three adjacent traps whereby a live-stained cell is secured in each. As can be noticed, cells remain intact and did not get damaged during trapping. Microcapillaries, demarcated by the dashed lines, are kept short (20 μm) so as to limit their electrical and hydrodynamic resistance and connected to suction ports through dedicated side microchannels. Figure 7(*c*) shows a relative per cent change in representative

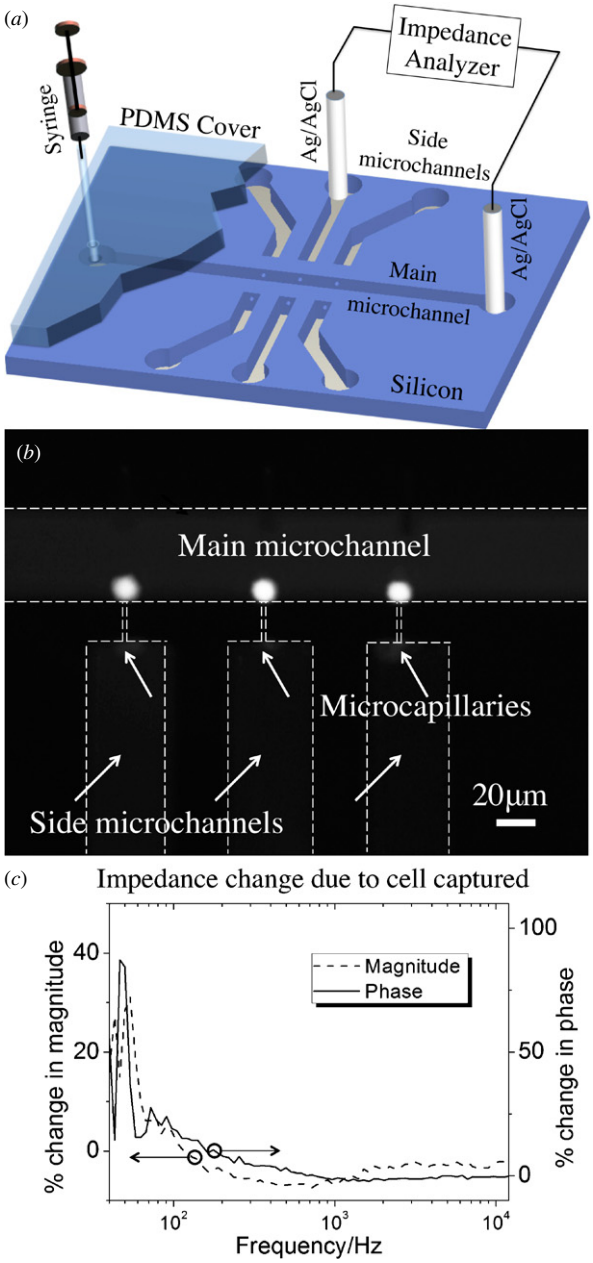

Figure 7. Probing biological cells for impedance spectroscopy through microcapillaries. (*a*) 3D rendering of the overall device and the measurement setup with the PDMS cover drawn incomplete for the clarity. (*b*) Fluorescent micrograph of a device presenting three identical microcapillaries 20 μm long and with dedicated side microchannels, probing live-stained cancer cells (HCT 116) delivered through main microchannel. (*c*) Representative change in magnitude and phase of impedance spectra across a microcapillary before and after capturing a cell.

impedance spectra recorded across a trap through external electrodes placed in respective ports before and after capturing a cell. The cell once occupies the trap causes a significant change in the impedance spectrum, ~30% in magnitude and ~85% in phase, particularly at low frequencies (<100 Hz). These values are in reasonable agreement with single-cell measurements obtained from various cell types using traps constructed through conventional fabrication techniques.

4. Conclusion

Surface migration of silicon atoms transforms ingeniously microstructured substrate topography into self-enclosed cylindrical microcapillaries based on the size and arrangement of a series of uniform rod-like trenches with submicrometer openings. Trenches placed on a 1D or 2D grid with a unit cell arranged in an equilateral triangle or square control the degree of surface porosity, the etched fraction of a unit cell, shown to be a good indicator for their ability to self-enclose into buried cavities under migration. Using the technique, straight microcapillaries, and microcapillaries with perpendicular turns and junctions can be produced. Selective removal of silicon around a point of interest along a silica microcapillary segment is proposed to enhance clarity and optical detection. Lastly, single-cell traps for impedance spectroscopy have been demonstrated based on the integration of short microcapillaries. Given the proof-of-concept demonstration of microcapillaries through silicon surface migration here, there is still plenty of room for improvement. First and foremost, the surface flatness of the substrate above the enclosed microcapillary should be recovered. This can be addressed by performing the anneal step in a low-pressure ambient and/or applying a smoothening step such as PSG reflow or chemical-mechanical planarization (CMP). Second, microcapillaries, although they are enclosed within the substrate, are considered surface structures and should be further distanced from the cover plate to allow cells more room and prevent their unnatural deformation. This can be achieved by epitaxial growth of silicon to elevate the substrate surface over the enclosed microcapillary prior to structuring reservoirs and large microchannels. Such additive technique (e.g. silicon epitaxy) could also be useful for building a 3D network of stacked microcapillaries if repeatedly applied in alternating sequence with the structuring of new trenches and their subsequent shape transformation under silicon surface migration. These strategies are currently being investigated.

Acknowledgments

Financial support for this project was provided in part by the Startup Grant from the ECE Department, HKUST, and the Research Grant Council of Hong Kong, a Direct Allocation grant to HKUST (no. DAG09/10.EG08).

References

[1] Whitesides G M 2006 The origins and future of microfluidics *Nature* **442** 368
[2] Seo J, Ionescu-Zanetti C, Diamond J, Lal R and Lee L P 2004 Integrated multiple patch-clamp array chip via lateral cell trapping junctions *Appl. Phys. Lett.* **84** 1973
[3] Ionescu-Zanetti C, Shaw R M, Seo J, Jan Y N, Jan L Y and Lee L P 2005 Mammalian electrophysiology on a microfluidic platform *Proc. Natl Acad. Sci. USA* **102** 9112
[4] Chen C and Folch A 2006 A high-performance elastomeric patch clamp chip *Lab Chip* **6** 1338
[5] Ong W L, Kee J S, Ajay A, Nagarajan R, Tang K C and Yobas L 2006 Buried microfluidic channel for integrated patch-clamping assay *Appl. Phys. Lett.* **89** 093902
[6] Ong W L, Tang K C, Agarwal A, Nagarajan R, Luo L W and Yobas L 2007 Microfluidic integration of substantially round glass capillaries for lateral patch clamping on chip *Lab Chip* **7** 1357
[7] Tang K C, Reboud J, Kwok Y L, Peng S L and Yobas L 2010 Lateral patch-clamping in a standard 1536-well microplate format *Lab Chip* **10** 1044
[8] Han A and Frazier A B 2006 Ion channel characterization using single cell impedance spectroscopy *Lab Chip* **6** 1412
[9] Cho S and Thielecke H 2007 Micro hole-based cell chip with impedance spectroscopy *Biosens. Bioelectron.* **22** 1764
[10] James C D, Reuel N, Lee E S, Davalos R V, Mani S S, Carroll-Portillo A, Rebeil R, Martino A and Apblett C A 2008 Impedimetric and optical interrogation of single cells in a microfluidic device for real-time viability and chemical response assessment *Biosens. Bioelectron.* **23** 845
[11] Chen J, Zheng Y, Tan Q, Zhang Y L, Li J, Geddie W R, Jewett M A S and Sun Y 2011 A microfluidic device for simultaneous electrical and mechanical measurements on single cells *Biomicrofluidics* **5** 014113
[12] Malleo D, Nevill J T, Lee L P and Morgan H 2010 Continuous differential impedance spectroscopy of single cells *Microfluid. Nanofluid.* **9** 191
[13] Khine M, Lau A D, Ionescu-Zanetti C, Seo J and Lee L P 2005 A single cell electroporation chip *Lab Chip* **5** 38
[14] Khine M, Ionescu-Zanetti C, Blatz A, Wang L-P and Lee L P 2007 Single-cell electroporation arrays with real-time monitoring and feedback control *Lab Chip* **7** 457
[15] Luo Y, Cao X, Huang P and Yobas L 2012 Microcapillary-assisted dielectrophoresis for single-particle positioning *Lab Chip* **12** 4085
[16] Sun Y, Kwok Y C and Nguyen N T 2007 Faster and improved microchip electrophoresis using a capillary bundle *Electrophoresis* **28** 4765
[17] Sun Y, Nguyen N T and Kwok Y C 2009 Enhanced electrophoretic DNA separation in photonic crystal fiber *Anal. Bioanal. Chem.* **394** 1707
[18] Cao Z, Ren K, Wu H and Yobas L 2012 Monolithic integration of fine cylindrical glass microcapillaries on silicon for electrophoretic separation of biomolecules *Biomicrofluidics* **6** 036501
[19] Kirby B J and Hasselbrink E F Jr 2004 Zeta potential of microfluidic substrates: part 1. Theory, experimental techniques, and effects on separations *Electrophoresis* **25** 187
[20] Kirby B J and Hasselbrink E F Jr 2004 Zeta potential of microfluidic substrates: part 2. Data for polymers *Electrophoresis* **25** 203
[21] Kim M-S, Cho S I, Lee K-N and Kim Y-K 2005 Fabrication of microchip electrophoresis devices and effects of channel surface properties on separation efficiency *Sensors Actuators* B **107** 818
[22] Lacher N A, de Rooij N F, Verpoorte E and Lunte S M 2003 Comparison of the performance characteristics of poly(dimethylsiloxane) and Pyrex microchip electrophoresis devices for peptide separations *J. Chromatogr.* A **1004** 225
[23] Madou M J 2002 *Fundamentals of Microfabrication: The Science of Miniaturization* (Boca Raton, FL: CRC Press)
[24] Lindner P, Dragoi V, Farrens S, Glinsner T and Hangweier P 2004 Advanced techniques for 3D devices in wafer-bonding processes *Solid State Technol.* **47** 55
[25] Fan Z H and Harrison D J 1994 Micromachining of capillary electrophoresis injectors and separators on glass chips and evaluation of flow at capillary intersections *Anal. Chem.* **66** 177

[26] Jacobson S C, Moor A W and Ramsey J M 1995 Fused quartz substrates for microchip electrophoresis *Anal. Chem.* **67** 2059
[27] Peeni B A, Conkey D B, Barber J P, Kelly R T, Lee L M, Woolley A T and Hawkins A R 2005 Planar thin film device for capillary electrophoresis *Lab Chip* **5** 501
[28] Turner S W, Perez A M, Lopez A and Craighead H G 1998 Monolithic nanofluid sieving structures for DNA manipulation *J. Vac. Sci. Technol.* B **16** 3835
[29] Chen J, Wise K D, Hetke J F and Bledsoe S C Jr 1997 A multichannel neural probe for selective chemical delivery at the cellular level *IEEE Trans. Biomed. Eng.* **44** 760–9
[30] de Boer M J, Tjerkstra R W, Berenschot J W, Jansen H V, Burger G J, Gardeniers J G E, Elwenspoek M and van den Berg A 2000 Micromachining of buried micro channels in silicon *J. Microelectromech. Syst.* **9** 94–103
[31] Rusu C *et al* 2001 Direct integration of micromachined pipettes in a flow channel for single DNA molecule study by optical tweezers *J. Microelectromech. Syst.* **10** 238–46
[32] Kaltsas G, Pagonis D N and Nassiopoulou A G 2003 Planar CMOS compatible process for the fabrication of buried microchannels in silicon using porous-silicon technology *J. Microelectromech. Syst.* **12** 863–72
[33] Barillaro G, Nannini A and Piotto M 2007 Electrochemical fabrication of buried folded microchannels into silicon substrates *Phys. Status Solidi* a **204** 1464–8
[34] Heuschkel M O, Guérin L, Buisson B, Bertrand D and Renaud P 1998 Buried microchannels in photopolymer for delivering of solutions to neurons in a network *Sensors Actuators* B **48** 356–61
[35] Chuang Y-J, Tseng F-G, Cheng J-H and Lin W-K 2003 A novel fabrication method of embedded micro-channels by using SU-8 thick-film photoresists *Sensors Actuators* A **103** 64–9
[36] Abbas A, Supiot P, Mille V, Guillochon D and Bocquet B 2009 Capillary microchannel fabrication using plasma polymerized TMDS for fluidic MEMS technology *J. Micromech. Microeng.* **19** 045022
[37] Sato N and Yonehara T 1994 Hydrogen annealed silicon-on-insulator *Appl. Phys. Lett.* **65** 1924–6
[38] Jeong S and Oshiyama A 1999 Complex diffusion mechanisms of a silicon adatom on hydrogenated Si(1 0 0) surfaces: on terraces and near steps *Surf. Sci.* **435** 481–5
[39] Sato T, Mitsutake K, Mizushima I and Tstrnashima Y 2000 Micro-structure transformation of silicon: a newly developed transformation technology for patterning silicon surfaces using the surface migration of silicon atoms by hydrogen annealing *Japan. J. Appl. Phys. 1* **39** 5033–8
[40] Mizushima I, Sato T, Taniguchi S and Tsunashima Y 2000 Empty-space-in-silicon technique for fabricating a silicon-on-nothing structure *Appl. Phys. Lett.* **77** 3290–2
[41] Sato T, Mizushima I and Tsunashima Y 2001 A new substrate engineering for the formation of empty space in silicon (ESS) induced by silicon surface migration *Trans. Inst. Elect. Eng. Japan* C **121** 524–9
[42] Kuribayashi H, Hiruta R, Shimizu R, Sudoh K and Iwasaki H 2003 Shape transformation of silicon trenches during hydrogen annealing *J. Vac. Sci. Technol.* A **21** 1279–83
[43] Kuribayashi H, Shimizu R, Sudoh K and Iwasaki H 2004 Hydrogen pressure dependence of trench corner rounding during hydrogen annealing *J. Vac. Sci. Technol.* A **22** 1406
[44] Lee M M and Wu M 2006 Thermal annealing in hydrogen for 3D profile transformation on silicon on insulator and sidewall roughness reduction *J. Microelectromech. Syst.* **15** 338–43
[45] Kanamori Y, Douzono K, Fujihira S and Hane K 2008 Development of a compact vacuum- and hydrogen-annealing machine for surface transformation of silicon and its applications to micro-optical devices *J. Vac. Sci. Technol.* A **26** 365–9
[46] Bermond J M, Métois J J, Egéa X and Floret F 1995 The equilibrium shape of silicon *Surf. Sci.* **330** 48
[47] Tanaka S, Bartelt N C, Umbach C C, Tromp R M and Blakely J M 1997 Step permeability and the relaxation of biperiodic gratings on Si(0 0 1) *Phys. Rev. Lett.* **78** 3342
[48] Kant R, Ferralis N, Provine J, Maboudian R and Howe R T 2009 Experimental investigation of silicon surface migration in low pressure nonreducing gas environments *Electrochem. Solid-State Lett.* **12** H437–40
[49] Aspnes D E 1999 *Optical Properties of Si: Properties of Crystalline Silicon* ed R Hull (London: INSPEC IEE) p 677
[50] Pumera M, Wang J, Opekar F, Jelinek I, Feldman J, Löwe H and Hardt S 2002 Contactless conductivity detector for microchip capillary electrophoresis *Anal. Chem.* **74** 1968–71
[51] Tey J N, Wijaya I P M, Wei J, Rodriguez I and Mhaisalkar S G 2010 Nanotubes-/nanowires-based, microfluidic-integrated transistors for detecting biomolecules *Microfluid. Nanofluid.* **9** 1185–214
[52] Kedzierskia J, Bokor J and Kisielowski C 1997 Fabrication of planar silicon nanowires on silicon-on-insulator using stress limited oxidation *J. Vac. Sci. Technol.* B **15** 2825–28
[53] Ligenza J R 1961 Effect of crystal orientation on oxidation rates of silicon in high pressure stream *J. Phys. Chem.* **65** 2011–14
[54] Schasfoort R B M, Schlautmann S, Hendrikse J and van den Berg A 1999 Field-effect flow control for microfabricated fluidic networks *Science* **286** 942–5
[55] Kalinina O, Lebedeva I, Brown J and Silver J 1997 Nanoliter scale PCR with TaqMan detection *Nucl. Acid Res.* 1999–2004